



ELSEVIER

Available online at www.sciencedirect.com

SCIENCE @ DIRECT®

International Journal of Rock Mechanics & Mining Sciences 41 (2004) 813–832

International Journal of
Rock Mechanics
and Mining Sciences

www.elsevier.com/locate/ijrmms

Dynamic stability analysis of jointed rock slopes using the DDA method: King Herod's Palace, Masada, Israel

Y.H. Hatzor^{a,*}, A.A. Arzi^b, Y. Zaslavsky^c, A. Shapira^d

^a Department of Geological and Environmental Sciences, Ben-Gurion University of the Negev, Beer-Sheva 84105, Israel

^b Geotechnical Consulting, 80 Krinizi st., Suite 23, Ramat-Gan 52601, Israel

^c Seismology Division, Geophysical Institute of Israel, Lod, Israel

^d The International Seismological Center, Pipers Lane, Berkshire RG194NS, UK

Accepted 19 February 2004

Abstract

A dynamic, two-dimensional, stability analysis of a highly discontinuous rock slope is demonstrated in this paper. The studied rock slope is the upper terrace of King Herod's Palace in Masada, situated on the western margins of the seismically active Dead Sea Rift. The slope consists of sub-horizontally bedded and sub-vertically jointed, stiff, dolomite blocks. The dynamic deformation of the slope is calculated using a fully dynamic version of DDA in which time-dependent acceleration is used as input.

The analytically determined failure modes of critical keyblocks in the jointed rock slope are clearly predicted by DDA at the end of the dynamic calculation. It is found however that for realistic displacement estimates some amount of energy dissipation must be introduced into the otherwise fully elastic, un-damped, DDA formulation. Comparison of predicted damage with actual slope performance over a historic time span of 2000 years allows us to conclude that introduction of 2% kinetic damping should suffice for realistic damage predictions. This conclusion is in agreement with recent results of Tsesarsky et al. (In: Y.H. Hatzor (Ed.), *Stability of Rock Structures: Proceedings of the Fifth International Conference of Analysis of Discontinuous Deformation*, Balkema Publishers, Lisse, 2002, pp. 195–203) who compared displacements of a single block on an inclined plane subjected to dynamic loading obtained by DDA and by shaking table experiments.

Using dynamic DDA it is shown that introduction of a simple rock bolting pattern completely stabilizes the slope.

© 2004 Elsevier Ltd. All rights reserved.

Keywords: Rock slope stability; DDA; Earthquake engineering; Site response; Damping

1. Introduction

In this paper, we apply a dynamic discontinuous deformation analysis (DDA) to a real jointed rock slope which has sustained a relatively well known record of earthquakes over the past 2000 years—the upper terrace of King Herod's Palace in Masada, situated along the western margins of the seismically active Dead Sea rift valley. Since we know the terrace has sustained tremors within a reasonably estimated range of intensity in documented historic events, we have a good constraint on dynamic DDA predictions, from the field. In particular, the amount of required energy dissipation in DDA, or “damping”, can be explored by comparing

DDA predictions with actual terrace performance over historic times. Thus, the amount of energy dissipation and related effects associated with shaking of a real jointed rock slope may be estimated, and the appropriate values can be used for realistic dynamic modeling of jointed rock slopes using DDA.

1.1. The numerical DDA

The DDA method [1], is similar in essence to the finite element method (FEM). It uses a finite element type of mesh but where all the elements are real isolated blocks, bounded by pre-existing discontinuities. DDA however is more general since blocks can be of any convex or concave shape. When the blocks are in contact Coulomb's law applies to the contact interface and the simultaneous equilibrium equations are formulated and

*Corresponding author. Tel.: +972-8-647-2621; fax: +972-8-647-2997.

E-mail address: hatzor@bgumail.bgu.ac.il (Y.H. Hatzor).

solved for each loading or time increment. In the FEM method the number of unknowns is the sum of the degrees of freedom of all nodes. In the DDA method the number of unknowns is the sum of the degrees of freedom of all the blocks. Therefore, from a theoretical point of view, the DDA method is a generalization of the FEM [2].

DDA considers both statics and dynamics using a time-step marching scheme and an implicit algorithm formulation. The difference between static and dynamic analysis is that the former assumes the velocity as zero in the beginning of each time step, while the latter inherits the velocity of the previous time step.

The formulation is based on minimization of potential energy and uses a “penalty” method to prevent penetration or tension between blocks. Numerical penalties in the form of stiff springs are applied at the contacts to prevent either penetration or tension between blocks. Since tension or penetration at the contacts will result in expansion or contraction of the springs, a process that requires energy, the minimum energy solution is one with no tension or penetration. When the system converges to an equilibrium state, however, there are inevitable penetration energies at each contact, which balance the contact forces. Thus, the energy of the penetration (the deformation of the springs) can be used to calculate the normal and shear contact forces.

Shear displacement along boundaries is modeled in DDA using the Coulomb–Mohr failure criterion. By adopting first-order displacement approximation the DDA method assumes that each block has constant stresses and strains throughout.

1.2. Basic mathematical formulation

For complete mathematical formulations refer to Shi [1,2]; here only the most basic equations are summarized. The displacements (u, v) at any point (x, y) in a block i can be related in two dimensions to six displacement variables:

$$D_i = (d_{1,i}, d_{2,i}, d_{3,i}, d_{4,i}, d_{5,i}, d_{6,i})^T = (u_0, v_0, r_0, \epsilon_x, \epsilon_y, \gamma_{xy})^T, \tag{1}$$

where (u_0, v_0) are the rigid body translations at a specific point (x_0, y_0) within the block, r_0 is the rotation angle of the block with a rotation center at (x_0, y_0), and ϵ_x, ϵ_y , and γ_{xy} are the normal and shear strains in the block. The complete first-order approximation of block displacements proves to take the following form [1,2]:

$$\begin{pmatrix} u \\ v \end{pmatrix} = [T_i][D_i], \tag{2}$$

where

$$[T_i] = \begin{bmatrix} 1 & 0 & -(y - y_0) & (x - x_0) & 0 & \frac{(y - y_0)}{2} \\ 0 & 1 & (x - x_0) & 0 & (y - y_0) & \frac{(x - x_0)}{2} \end{bmatrix}. \tag{3}$$

This equation enables the calculation of displacements at any point (x, y) within the block when the displacements are given at the center of rotation and when the strains (constant within the block) are known. In the two-dimensional formulation, the center of rotation with coordinates (x_0, y_0) coincides with the block centroid with coordinates (x_c, y_c). Assuming n blocks constitute the block system, the simultaneous equilibrium equations are written in a matrix form as follows:

$$\begin{bmatrix} K_{11} & K_{12} & K_{13} & \cdot & \cdot & \cdot & K_{1n} \\ K_{21} & K_{22} & K_{23} & \cdot & \cdot & \cdot & K_{2n} \\ K_{31} & K_{32} & K_{33} & \cdot & \cdot & \cdot & K_{3n} \\ \cdot & \cdot & \cdot & \cdot & \cdot & \cdot & \cdot \\ \cdot & \cdot & \cdot & \cdot & \cdot & \cdot & \cdot \\ \cdot & \cdot & \cdot & \cdot & \cdot & \cdot & \cdot \\ K_{n1} & K_{n2} & K_{n3} & \cdot & \cdot & \cdot & K_{nn} \end{bmatrix} \begin{bmatrix} D_1 \\ D_2 \\ D_3 \\ \cdot \\ \cdot \\ \cdot \\ D_n \end{bmatrix} = \begin{bmatrix} F_1 \\ F_2 \\ F_3 \\ \cdot \\ \cdot \\ \cdot \\ F_n \end{bmatrix}, \tag{4}$$

where each coefficient K_{ij} is defined by the contacts between blocks i and j . Since each block (i) has six degrees of freedom defined by the components of D_i above, each K_{ij} is in itself a 6×6 sub-matrix. Also, each F_i and D_i are 6×1 sub matrices where D_i represents the deformation variables ($d_{1i}, d_{2i}, d_{3i}, d_{4i}, d_{5i}, d_{6i}$) of block i , and F_i is the loading on block i distributed to the six deformation variables. Sub matrix $[K_{ij}]$ depends on the material properties of block i and $[K_{ji}]$, where $i \neq j$, is defined by the contacts between block i and j .

The system of equations above (4) can also be represented in a more compact form as $\mathbf{KD} = \mathbf{F}$ where \mathbf{K} is a $6n \times 6n$ stiffness matrix and \mathbf{D} and \mathbf{F} are $6n \times 1$ displacement and force vectors, respectively. Hence, in total, the number of displacement unknowns is the sum of the degrees of freedom of all the blocks. Note that in essence the system of equations (4) is similar in form to that in the FEM [3].

The solution of the system of equations is constrained by the system of inequalities associated with block kinematics (no penetration and no tension between blocks) and Coulomb friction for sliding along block interfaces, which is the main source of energy consumption. The final displacement variables for a given time step are obtained in an iterative process (see [1–3] for details).

The equilibrium equations [1,2] are established by minimizing the total potential energy Π produced by the forces and stresses. The i th row of Eq. (4) consists of six

linear equations:

$$\frac{\partial \Pi}{\partial d_{ri}} = 0, \quad r = 1 \rightarrow 6, \quad (5)$$

where the d_{ri} is the deformation variable of block i . For block i the equations:

$$\frac{\partial \Pi}{\partial u_0} = 0, \quad \frac{\partial \Pi}{\partial v_0} = 0 \quad (6)$$

represent the equilibrium of all the loads and contact forces acting on block i along x and y directions, respectively. The equation:

$$\frac{\partial \Pi}{\partial r_0} = 0 \quad (7)$$

represents the moment equilibrium of all the loads and contact forces acting on block i . The equations:

$$\frac{\partial \Pi}{\partial \varepsilon_x} = 0, \quad \frac{\partial \Pi}{\partial \varepsilon_y} = 0, \quad \frac{\partial \Pi}{\partial \gamma_{xy}} = 0 \quad (8)$$

represent the equilibrium of all external forces and stresses on block i along x, y .

The total potential energy Π is the summation over all potential energy sources, that is individual stresses and forces. The details for forming the sub-matrices K_{ij} and F_i in Eq. (4) for elastic stresses, initial stresses, point loads, volume forces, bolting forces, inertia forces, and viscosity forces, are provided by Shi [1,2]. An excellent review of DDA within the framework of other numerical methods in rock mechanics is provided by Jing [4].

In this research a new C/PC version of DDA is used [5] where earthquake acceleration can be input directly in every time step. A necessary condition for direct input of earthquake acceleration is that the numerical computation has no artificial damping, because damping may reduce the earthquake dynamic energy thus under estimating the damage. In DDA the solution of the equilibrium equations is performed without damping and therefore DDA should be a suitable method for the task of a fully dynamic analysis in jointed rock masses. Nevertheless, as will be discussed below, we suggest here that some amount of energy dissipation must be introduced into the otherwise fully un-damped formulation of DDA, if realistic displacement predictions are sought.

1.3. Dynamic DDA validation using analytical solutions

Before we attempt to apply dynamic DDA to a full-scale problem of a jointed rock slope it is necessary to check whether dynamic DDA displacements are matched by analytical solutions. Hatzor and Feintuch [6] demonstrated the validity of DDA results for fully dynamic analysis of a single block on an incline subjected to dynamic loading. DDA runs were performed without introduction of any damping, as in the analytical solution. First, following previous work by

MacLaughlin [7], the dynamic solution for a single block on an incline subjected to constant gravitational acceleration was repeated using the new version of DDA [5]. For a slope inclination of 22.6° , four dynamic displacement tests were performed for interface friction angle values of $5^\circ, 10^\circ, 15^\circ$, and 20° . The agreement between the analytical and DDA solutions was within 1–2%. Next, Hatzor and Feintuch investigated three different sinusoidal functions of increasing complexity for the dynamic load input function, and checked the agreement between DDA and the derived analytical solutions. A good agreement between the analytical solution and DDA was obtained in all cases (see example in Fig. 1 for the function $a_t = 2\sin t + 3\sin 3t$).

1.4. Dynamic DDA validation using shaking table experiments

Wartman et al. [8] studied the dynamic displacement problem of a block on an incline using shaking table experiments that were performed at the U.C. Berkeley Earthquake Engineering Laboratory. Following Wartman's experimental work Tsesarsky et al. [9] repeated identical tests numerically using DDA. A representative result is shown in Fig. 2 for a sinusoidal input function with frequency of 2.66 Hz and interface friction angle of 16° . The DDA output is shown in symbols for four values of energy dissipation ($k01$): 0%, 1.5%, 2%, and 2.5%. For 0% dissipation ($k01 = 1.0$) the velocity of each block at the end of a time step is completely transferred to the beginning of the following time step. For 1.5% dissipation ($k01 = 0.985$) the initial velocity of a time step is 1.5% smaller than the terminal velocity of the previous time step.

The results of Tsesarsky et al. [9] show that with zero energy dissipation ($k01 = 1.0$) DDA results overestimate the physical displacements by as much as 80%. With as little as 2% dissipation however ($k01 = 0.98$) DDA displacements match the physical test results within 5% accuracy. This finding suggests that realistic application of dynamic DDA must incorporate some

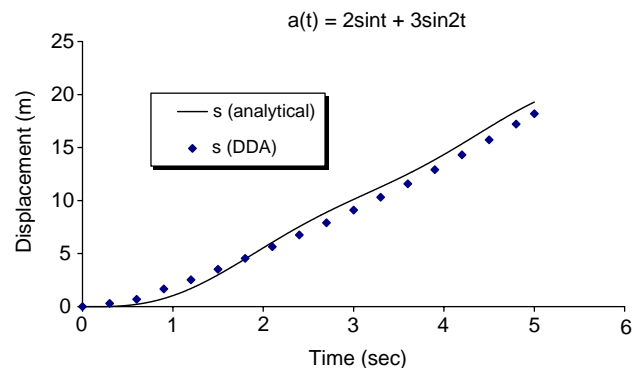


Fig. 1. Validation of dynamic DDA using analytical solutions (after Hatzor and Feintuch [6]).

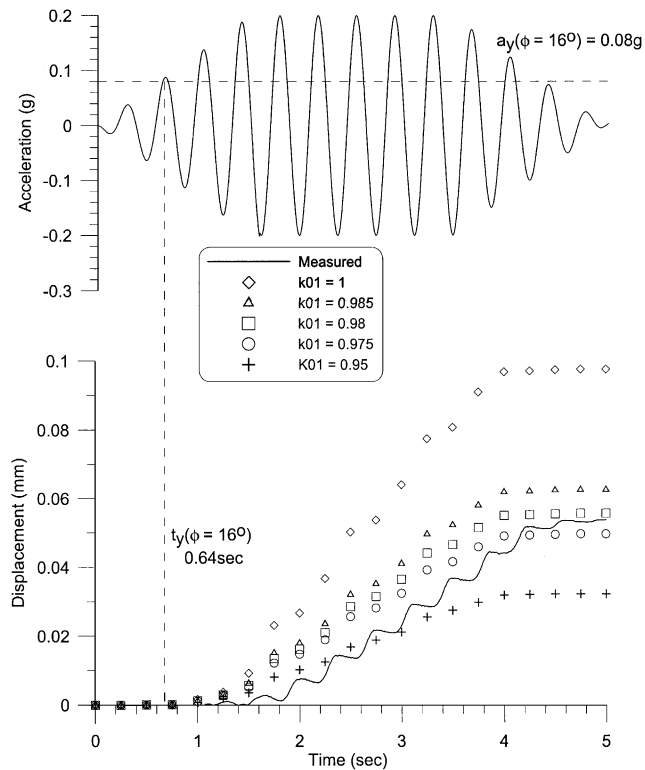


Fig. 2. Validation of dynamic DDA using shaking table experiments [9]: Top—sinusoidal input function of 2.66 Hz frequency; bottom—comparison between measured physical displacement and DDA solution with various levels of kinetic damping (plane inclination 11.37° , interface friction angle 16° , block elastic modulus $E = 5 \times 10^9 \text{ N/m}^2$, numeric spring stiffness $g_0 = 5 \times 10^8 \text{ N/m}$, time step size $g_1 = 0.0025 \text{ s}$, assumed maximum displacement ratio $g_2 = 0.005$).

form of energy dissipation in order to account for energy loss mechanisms that are not modeled by DDA. Examples for such energy dissipation mechanisms may be block fracture at contact points, contact surface damage during slip, etc.

The shaking table validation [9] pertains to a single block on an incline. McBride and Scheele [10] studied a multi-block toppling problem using a slope with a stepped base consisting of 50 blocks. Their conclusion was that as much as 20% energy dissipation was required in order to obtain realistic agreement between the physical model and DDA. Perhaps better conditioning of the numeric control parameters in [10] would have reduced the required amount of energy dissipation in the validation study.

2. Geological and seismological setting of Herod's Palace, Masada

The top of Mount Masada consists of essentially bare hard rocks. The rocks are mainly bedded limestone and dolomite, with near vertical jointing. Structurally, the

entire mountain is an uplifted block within the band of faults which forms the western boundary of the Dead Sea Rift, a seismically active transform [11,12]. A review of the tectonics and seismicity of the area is provided by Niemi et al. [13]. According to the Israel building code—Israel Standard 413, the Dead Sea valley has been classified as a region in which earthquake-induced peak horizontal ground acceleration (PGA) exceeding $0.2g$ at the bedrock level is expected with a 10% probability within any 50 year windows. This is analogous to a 475-year average recurrence interval for such acceleration. In this paper we repeatedly refer to PGA for simplicity, which is adequate in the present context, although PGA is not necessarily the best measure of the seismic hazard (e.g. [14,15]).

Inspection of the historic earthquake record [16–18] suggests that the strongest shaking events which have actually affected Mount Masada within the past 2000 years, were due to about ten identified earthquakes with estimated magnitudes in the range of 6.0 ± 0.4 and focal distances probably in the order of several kilometers to a few tens of kilometers from the site. With these parameters, it is highly likely that some of these earthquakes have caused at Mount Masada bedrock PGA's reaching and even exceeding $0.2g$, in general agreement with predictions for a 2000 year period based on the aforementioned building code assumptions.

One of the most notable historic earthquakes in this region occurred probably in the year 362 or 363, with a magnitude estimated at 6.4 [16] or even 7.0 [17]. Reported effects included seismic seiches in the Dead Sea and destruction in cities tens of kilometers from the Dead Sea, both east and west. This is probably the earthquake identified by archeologists as “the great earthquake which destroyed most of the walls on Masada sometime during the second to the fourth centuries” [19]. The most recent of the major historic earthquakes near Mount Masada occurred on 11 July 1927. This earthquake was recorded by tens of seismographs, yielding a magnitude determination of 6.2 and an epicenter location $30 \pm 10 \text{ km}$ north of Masada. It also caused seismic seiches in the Dead Sea and destruction in cities tens of kilometers away [15].

2.1. Observed historical stability

The fortifications built by King Herod on Mount Masada about 2000 years ago included a casemate wall surrounding the relatively flat top of the mountain [19]. Clearly, because of its defensive function, the outer face of this wall was built so as to continue upward the face of the natural cliff, as much as possible. The outer wall was therefore founded typically on the flat top within several decimeters from its rim. Locally it was even founded slightly beyond the rim, on a somewhat lower ledge of rock. On the aforementioned three palace

terraces, jutting at the northern tip of the mountain top, construction was again carried out up to the rim and beyond in order to achieve architectural effects and utilize fully the limited space. Thus, the remaining foundations effectively serve to delineate the position of the natural rim of the flat mountain top and associated northern terraces about 2000 years ago. Missing portions along such foundation lines indicate locations in which the rim has most probably receded due to rockfalls, unless the portions are missing due to other obvious reasons such as local erosion of the flat top by water or an apparent location of the foundation on fill beyond the rim.

Our inspection of the entire rim of the top of Masada reveals that over almost the entire length of the casemate wall, which is about 1400 m, the rock rim has not receded during the past 2000 years more than a few decimeters, if at all. Only over a cumulative total of less than 40 m, i.e. about 3% of the wall length, there are indications of rockfalls involving rim recessions exceeding 1.5 m, but not exceeding 4.0 m. Since the height of the nearly vertical cliffs below the rim is in the order of tens of meters, these observations attest to remarkable overall stability in the face of the recurring earthquakes.

On King Herod’s palace terraces there has been apparent widespread destruction, mostly of walls and

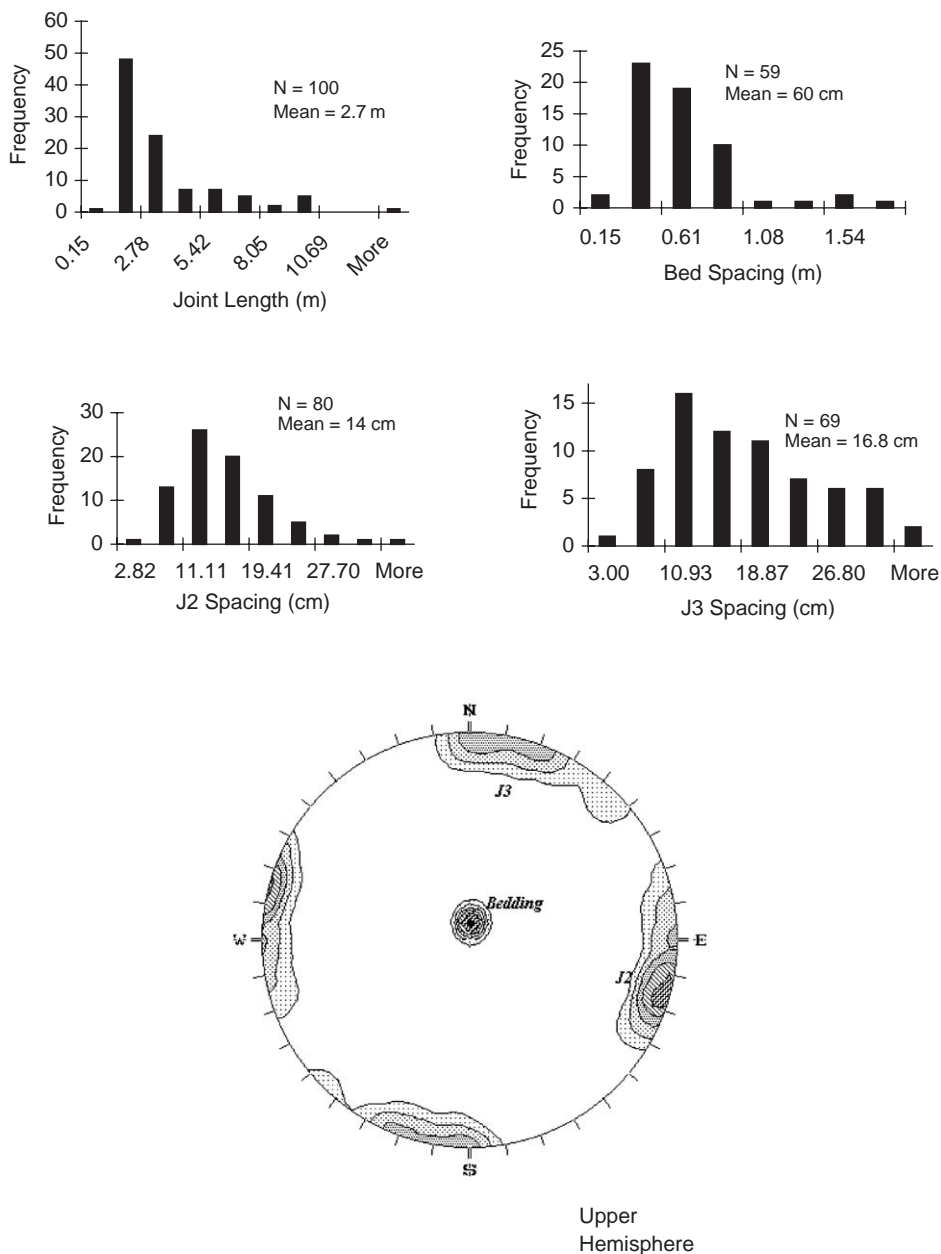


Fig. 3. Discontinuity length, spacing, and orientation distribution at the foundations of King Herod’s Palace, Masada. Upper Hemisphere projection of poles.

fills which were somehow founded on the steep slopes. However, in the natural cliffs themselves there are few indications of rockfalls involving rim recessions of more than a few decimeters. Remarkably, most of the high retaining walls surrounding the middle and lower terraces are still standing, attesting to the stability of the rock behind them. In the upper terrace, on which this study is focused, there appears to be only one rockfall with depth exceeding several decimeters. It is a local rockfall near the top of the 22 m cliff, in the northeast, causing a rim recession of about 2.0 m. It is notable that this particular section of the terrace cliff was substantially modified by the palace builders, perhaps de-stabilizing the pre-existing natural cliff.

We have also inspected rare aerial photographs of Mount Masada dated 29 December 1924, i.e. predating the 1927 earthquake. Our comparison with recent aerial photographs would have been capable of detecting rim recessions exceeding about 1 m, if any had occurred in the northern part of the mountain. None were found, suggesting that the 1927 earthquake did not cause any significant rockfalls there (the southern part was less clear in the old photographs).

The information presented above essentially constitutes results of a rare rock-mechanics field-scale “experiment”. Two thousand years ago the Masada cliff top was marked by construction. The mountain was later shaken by several major earthquakes, with deep bedrock accelerations certainly exceeding $0.1g$ and probably even exceeding $0.2g$. Observations at the present stage of the “experiment” show that all the cliffs surrounding the top of Mount Masada essentially withstood the shaking, with some relatively minor rockfalls at the top of the cliffs.

The above is a substantial result of a full-scale “experiment” on the real rock structure. Therefore, a fundamental test of any model of this structure is that it must essentially duplicate the above “experiment”. As shown in the sequel, we subjected our DDA model to this test, obtaining instructive results.

2.2. Topographic site effect at Masada

The eastern slope of Masada creates a steep drop of more than 250 m between the mountaintop and the rift valley floor. The resulting topography calls for a possible topographic site effect at Masada. Theoretical considerations of topographic site effect and its influence on surface ground motion were observed and studied by many authors [20–25]; simulations of topographic amplifications have been performed using various theoretical methods [26,27]. These studies show that amplification up to factor ten and more can be expected at the ridge top.

In order to assess the topography effect at the site four seismic stations were deployed during 10–13

September 1998 at the top (stations 1 and 2), mid-section (station 3), and foot (station 4) of the mountain. Fig. 4 shows a map of the study area, topographic profiles and the locations of the seismic stations. The recorded data consist of several windows of microtremors and one earthquake. Ground motion amplification was estimated by three spectral ratio methods: (a) conventional reference station technique, (b) receiver function estimates based on earthquake data, and (c) the Nakamura method using data of ambient seismic noise [28]. Fig. 5 shows individual and average horizontal-to-vertical spectral ratios for Sites 1 and 2 obtained from microtremors. The dominant feature of all spectral ratios is the high spectral ratio level at a frequency of about 1.4 Hz. At this frequency we also observe differences between the EW and NS components. Such differences are characteristic of topography effects. At the summit of Mt. Masada, the average spectral ratios reach maxima of about 2.5 in the EW direction and about 2 in the NS direction. We should point out here that the Nakamura method provides, in general, a relatively reliable estimate of the predominant frequency of the site (resonance frequency) but it is less reliable for

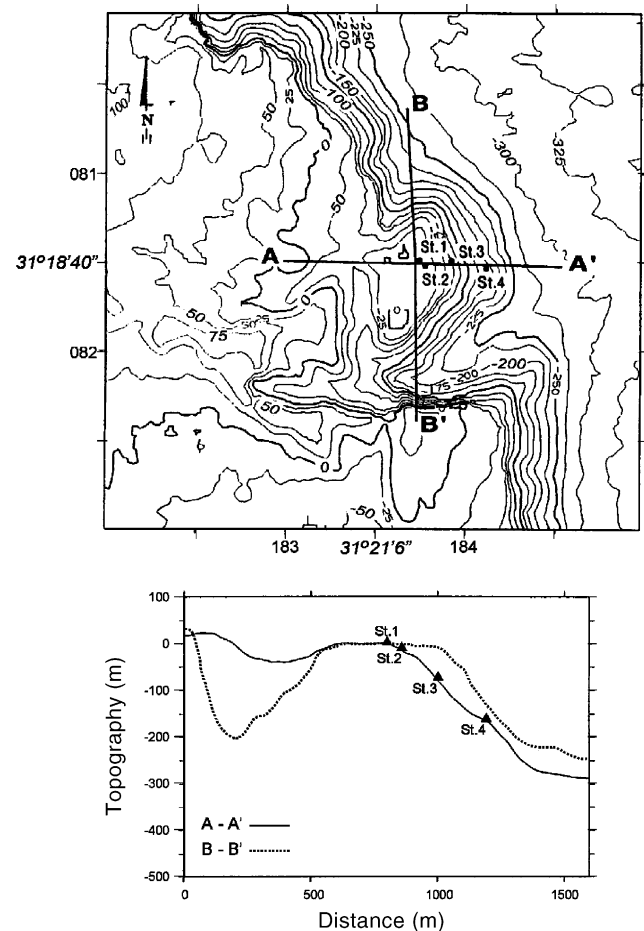


Fig. 4. Topographic map and profiles along sections A and B of Mt. Masada.

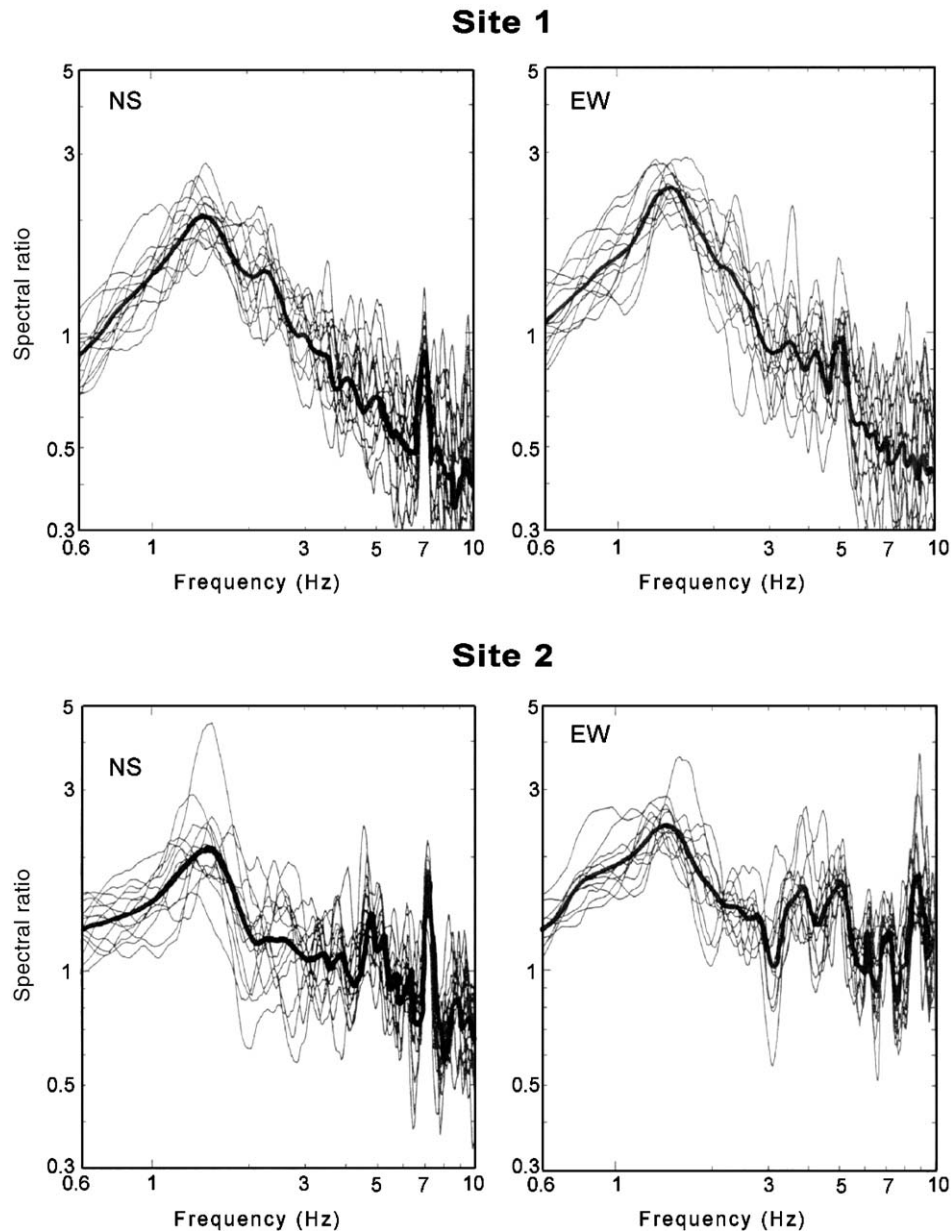


Fig. 5. Individual and average (heavy lines) horizontal-to-vertical spectral ratios for Mt. Masada obtained from micro-tremors recorded at Sites 1 and 2.

estimating the amplification level, especially at other frequencies. Fig. 6 shows spectral ratios for Sites 1 and 2 with respect to reference Site 4. These are calculated from seismic waves of an earthquake (southeast Cyprus, 13 October 1998 at 12:28, $M_L = 2.9$; the epicentral distance is 545 km). There are only small variations in the site response of the two sites. The ratios show a prominent peak at about 1.3 Hz. Here the horizontal ground motion oriented EW is amplified by a factor of about 3.5, while it is about 2.0 in the NS direction, i.e., Mt. Masada exhibits a preferential direction of resonance motion. Plotted in Fig. 7 are the horizontal-to-vertical spectral ratios for Sites 1 and 2 for the S-wave window (receiver function). Again, the receiver function

clearly exhibits the resonant peak in the frequency range 1.2–1.4 Hz with amplification values of about 3.5. Fig. 8a shows the horizontal-to-vertical spectral ratios for the NS component obtained from microtremors at Site 3. As shown, the average Nakamura site response estimate has a predominant peak near 1.4 Hz with amplification up to 2.2. Another dominant feature of the average spectral ratio is the high in the frequency range near 6 Hz. Fig. 8b presents spectral ratios calculated from the earthquake near Cyprus with respect to reference Site 4. The main differences between Sites 1, 2 and 3 are in the frequency band at about 1.4–1.8 Hz and about 4.0–5.0 Hz. For Site 3, the average spectral ratio obtained by the reference station shows a

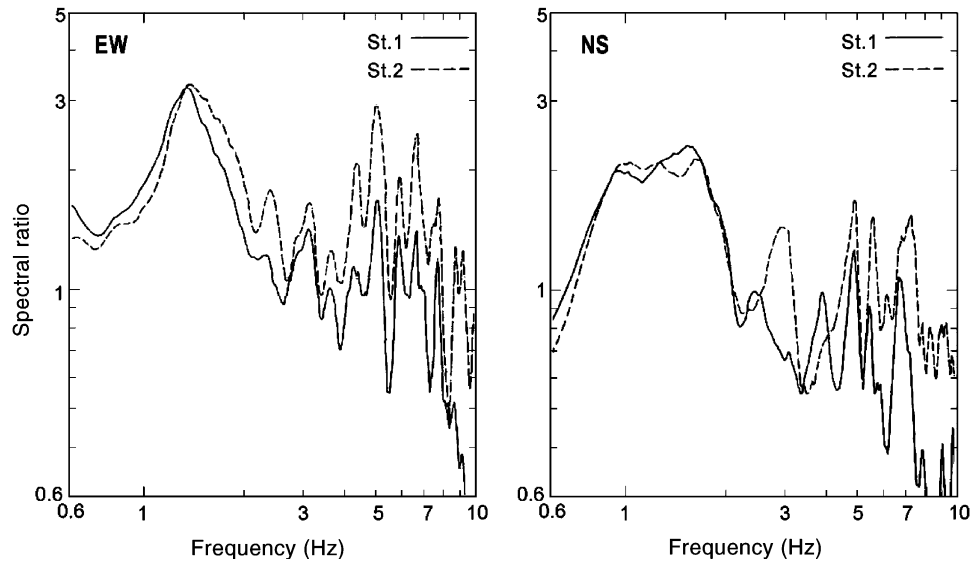


Fig. 6. Spectral ratios for Sites 1 and 2 at Mt. Masada computed from earthquake with respect to Site 4.

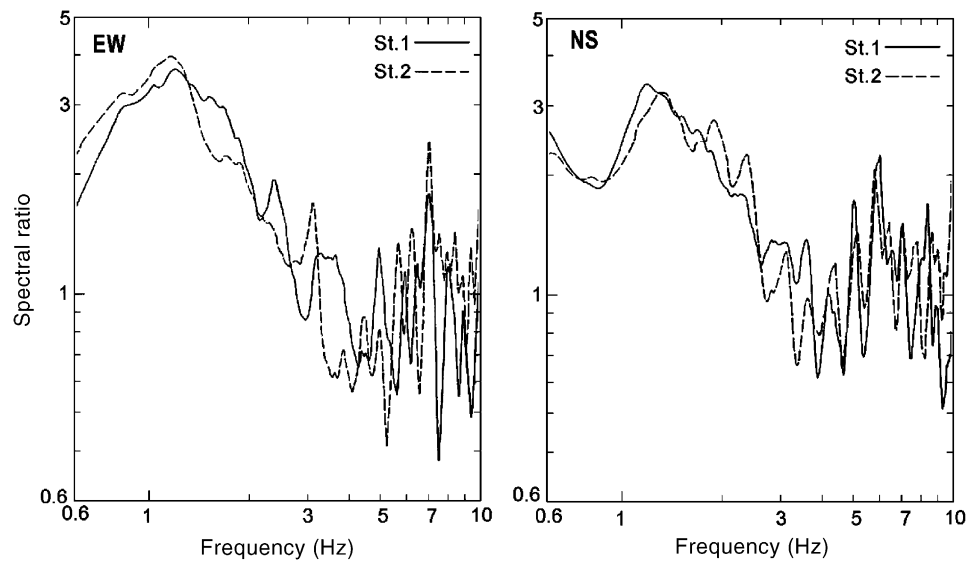


Fig. 7. Horizontal-to-vertical spectral ratios obtained from earthquake data for Sites 1 and 2 at Mt. Masada.

prominent peak near 1.4 Hz with amplification of only 2.0 whereas at about 4.0 Hz the amplification factor is about 4.0.

The site response obtained at Mt. Masada with respect to the reference station shows a well-defined peak at about 1.4 Hz. The horizontal ground motion oriented EW is amplified by a factor up to 3.5. Similarly, this peak is present in the receiver functions and in the average horizontal-to-vertical spectral ratios of micro-tremors. If the amplification effect is caused by topography, the frequency involved should correspond to a wavelength equivalent to the horizontal relief dimension [29], which here is about 1300 m (see Fig. 4).

Assuming an S-wave velocity of 1400 m/s for the uppermost layer of Mt. Masada [30], we should expect the topographical effects to be observed in the frequency of 1.1 Hz, in arguable agreement with the experiment.

3. Mechanical properties

The rock in Masada is a massive and dense dolomite with low porosity (2–8%) and density of 2730 kg/m³. The rock mass is bedded with local karstic voids between beds. The bedding planes are generally clean and tight, with crushed dolomite infilling in places.

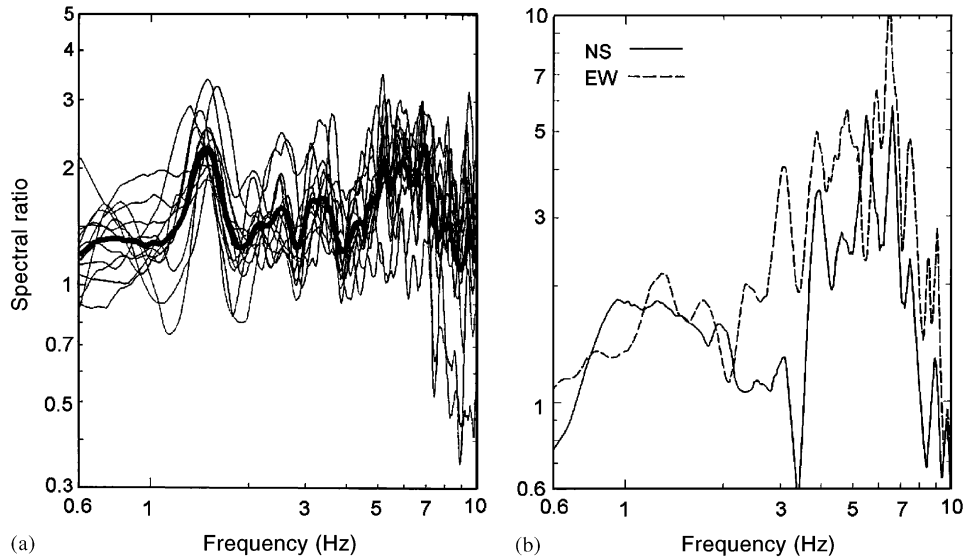


Fig. 8. (a) Horizontal-to-vertical spectral ratios from micro-tremors (EW component); and (b) spectral ratios to Site 4 from an earthquake; all for Site 3 at Mt. Masada.

Table 1
Discontinuity data for the foundations of King Herod’s Palace—Masada

Set #	Discontinuity type	Dip	Spacing (m)	Cohesion, (MPa)	ϕ (°)
1	Bedding	5/N	0.60	0	41
2	Joints	80/ESE	0.14	0	41
3	Joints	80/NNE	0.17	0	41

3.1. Rock mass structure

Herod’s palace, also known as the North palace, is built on three terraces at the north face of Masada. The rock mass structure at the foundations consists of two orthogonal, sub-vertical, joint sets striking roughly parallel and normal to the NE trending axis of the mountain, and a set of well developed bedding planes gently dipping to the north (Table 1). The joints are persistent, with mean length of 2.7 m. The bedding planes, designated here as J_1 , dip gently to the north with mean spacing of 60 cm. The two joint sets, J_2 and J_3 , are closely spaced with mean spacing of 14 and 17 cm, respectively (Fig. 3).

3.2. Strength and elasticity of intact rock

The elastic behavior of the rock was studied using a stiff, hydraulic, closed-loop servo controlled load frame with maximum axial force of 1.4 MN, and stiffness of 5×10^9 N/m (Terra-Tek model FX-S-33090). The testing procedures are described elsewhere [31]. The uniaxial compressive strength of intact rock samples exceeds 315 MPa, and typical values of elastic modulus and Poisson’s ratio are 40 GPa and 0.18, respectively. These strength and elasticity parameters are relatively high

with respect to values determined experimentally for other dolomites and limestones in Israel [32,33].

3.3. Shear strength of discontinuities

The residual friction angle of joints was determined using tilt tests performed on saw-cut and ground surfaces of dolomite, assuming the joint planes are clean and tight. Twenty tilt tests performed on saw-cut and ground surfaces provided a mean friction angle of 28° and 23°, respectively. The 5° difference is attributed to roughness resulting from saw-cutting operations.

The shear strength of filled bedding planes was determined using a segment triaxial test performed on a right cylinder containing an inclined saw cut plane at 35° to the axis of the cylinder, filled with crushed dolomite. Seven different segments were performed, with confining pressure values ranging between 2.2 and 16.2 MPa. A linear Coulomb–Mohr failure criterion was found, with zero cohesion and a residual friction angle of 22.7° [34]. The similarity between the results of tilt tests on ground surfaces (23°) and the segment triaxial test on a filled saw-cut plane (22.7°) suggests that during shear the infilling material crushed all remaining asperities in the saw-cut sample resulting in a failure envelope representing residual conditions. The residual

friction angle value of 23° may therefore be applicable for very large blocks where some initial shear displacements have already taken place due to historic cycles of seismic loading [34]. However, for dynamic analysis of smaller blocks with high static factor of safety the strengthening effect of initial asperities ought to be considered.

The shear strength of rough bedding planes was determined using real bedding plane samples from the foundations of the North palace. The upper and lower sides of the mating planes were kept in contact with no disturbance and were transported to the lab at natural water content. The two samples were cast inside two $200 \times 200 \times 150 \text{ mm}^3$ shear boxes while the mating surfaces were kept intact. The gap between the rock and the box frame was filled with Portland cement.

Direct shear tests were performed using a hydraulic, close loop servo-controlled, direct shear system with normal force capacity of 1000 kN and horizontal force capacity of 300 kN (Product of TerraTek Systems Inc.). The stiffness of the normal and shear load frames is 7.0 and 3.5 MN/m, respectively. Normal and horizontal displacement during shear were measured using four and two 50 mm LVDTs with 0.25% linearity full scale. Axial load was measured using a 1000 kN capacity load cell with 0.5% linearity full scale. Shear load was measured using a 300 kN load cell with 0.5% linearity full scale. Two segment direct shear tests were performed (samples MNP3, MNP4) under a constant shear displacement rate of 1 mil/s (0.025 mm/s) and under an imposed constant normal stress condition.

In Fig. 9 shear stress vs. shear displacement is shown for sample MNP-3 that was loaded, unloaded, and reloaded in eight cycles of increasing normal stress from 0.17 to 1.38 MPa. In each cycle the sample was sheared forward, in the first cycle a distance of 1.3 mm, and then additional 0.5 mm of forward shear displacement in each consecutive segment. Plotting the peak shear stress vs.

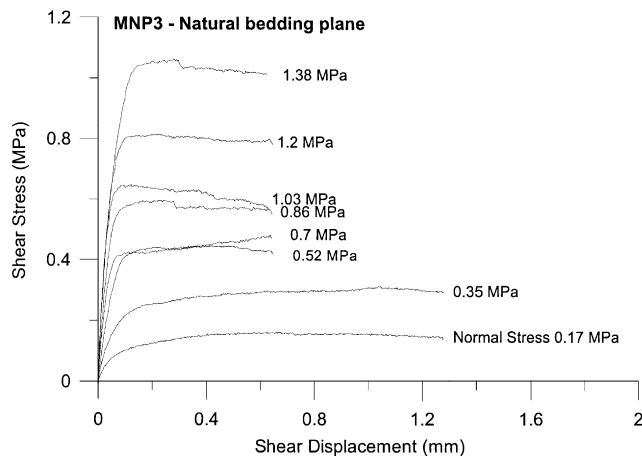


Fig. 9. Results of a segment direct shear test performed on a natural bedding plane sample from Masada.

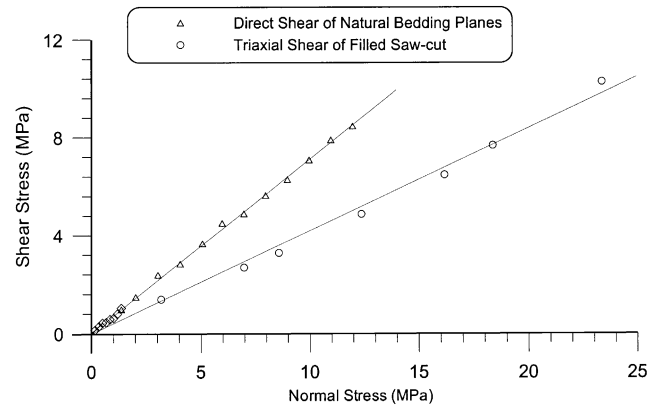


Fig. 10. Failure envelope of rough (Δ) and smooth (\circ) bedding planes in Masada dolomites.

normal load for the two segment tests (open triangles in Fig. 10) reveals a bilinear failure envelope:

$$0 < \sigma_n < 0.5 \text{ MPa} : \tau = 0.88 \sigma_n (R^2 = 0.999),$$

$$0.5 < \sigma_n \leq 12 \text{ MPa} : \tau = 0.083 + 0.71 \sigma_n (R^2 = 0.998). \quad (9)$$

These results indicate that for low normal load (up to 0.5 MPa) the peak friction angle for the bedding planes at Masada is 41.3° . For higher normal loads the peak friction angle reduces to 35.3° . The residual friction angle value is determined from the triaxial test results [34] as 23° (open circles in Fig. 10).

The maximum height of the terrace at the North Palace is 25 m and therefore the normal stress acting on bedding planes at the site cannot be greater than 682 kPa. Therefore, in light of the experimental results, the low normal load criterion is used for analysis with a peak friction angle value of 41° .

4. Block system mesh generation

The results of numerical analyses are extremely sensitive to: (a) the input mechanical and physical properties, (b) the geometrical configuration, namely the computed mesh, and (c) the input loading function. The geometrical configuration (b) is particularly important in distinct element methods where rock blocks and mesh elements are one and the same. In the previous section the determination of mechanical parameters was discussed. In this section the most suitable mesh configuration is discussed, followed by a discussion of the appropriate dynamic input motion.

Two principal joint sets and a systematic set of bedding planes comprise the rock structure at Herod's palace (Fig. 3). An E–W cross section of the upper terrace is shown in Fig. 11, computed using the statistical joint trace generation code (DL) of Shi [1,2]. It can be seen intuitively that while the East face of the rock terrace is prone to sliding of wedges, the West face

is more likely to fail by toppling of individual blocks. Block theory mode and removability analyses [35] confirm these intuitive expectations.

While it is quite convenient to use mean joint set attitude and spacing to generate statistically a synthetic mesh, the resulting product (Fig. 11) is quite unrealistic and bears little resemblance to the actual slope. The contact between blocks obtained this way is planar, thus interlocking between blocks is not modeled. Consequently the results of dynamic calculations may be overly conservative and the computed displacements unnecessarily exaggerated. This indeed was the result of several dynamic analysis runs performed in the past for this particular problem [36,37].

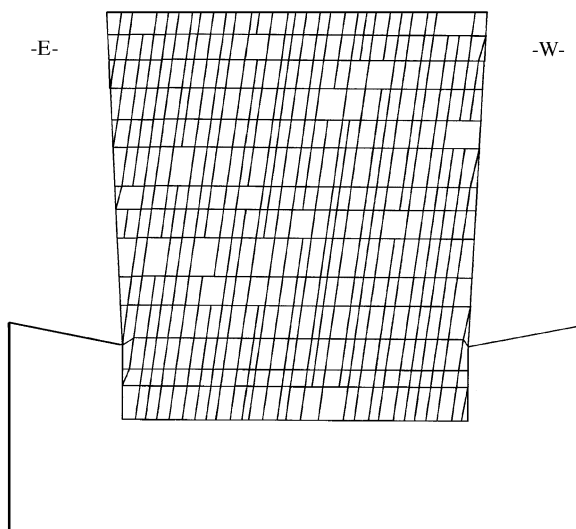


Fig. 11. Synthetic trace map of the upper rock terrace of Herod's Palace in Masada using the statistical joint trace generation code (DL) of Shi [1].

In order to analyze the dynamic response of the slope realistically a photo-geological trace map of the face was prepared using aerial photographs (Fig. 12), and the joint trace lines were digitized. Then, the block-cutting (DC code) algorithm of Shi [1,2] was utilized in order to generate a trace map that represents more closely the reality in the field (Fig. 13). Inspection of Fig. 13 reveals that block interlocking within the slope is much higher and therefore the results of the forward analysis are expected less conservative but more realistic. The deterministic mesh shown in Fig. 13 is used therefore in the forward modeling discussed below.

5. Input motions

5.1. The significance of the selected input motion

The determination of mechanical input parameters is straightforward in the case of strong and stiff rocks with clean discontinuities as in the case of Masada. The determination of the correct geometrical configuration involves a measure of geological engineering judgment, but nevertheless can be established quite accurately once a sound structural model for the rock mass is put together. The selection of the most suitable input motion for forward dynamic modeling is not a simple task, however, as it involves subjective judgment with respect to the most characteristic earthquake for the particular site at hand, and with respect to the relative significance of local site effects.

Determination of the most relevant input motion will prove very beneficial in terms of computation (CPU) time required for the analysis. In fully dynamic analysis performed in time domain, application of a time-step

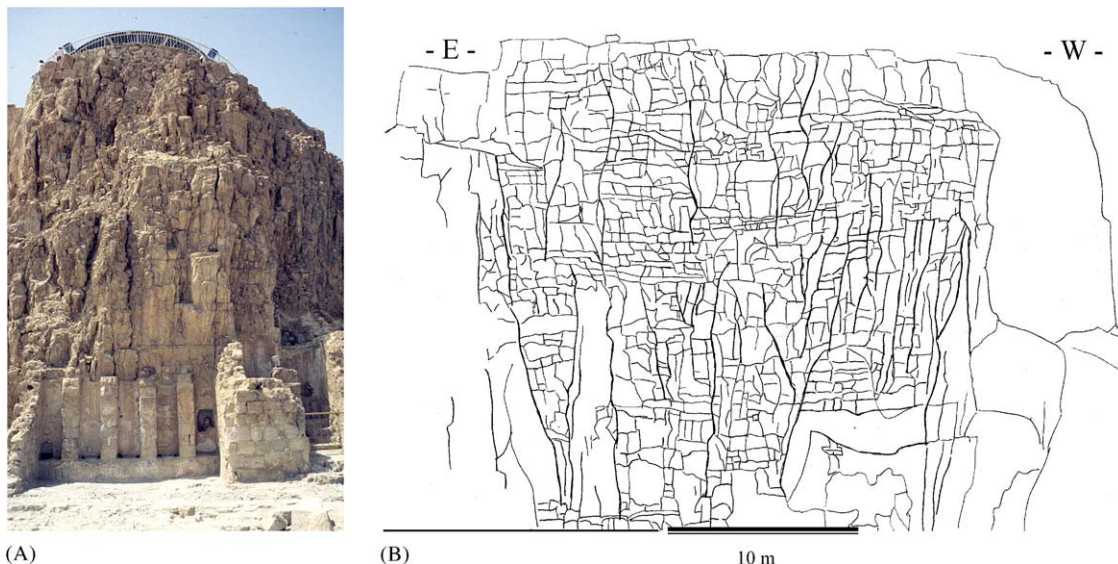


Fig. 12. (A) The upper terrace of Herod's palace, Masada; and (B) photo geological trace map.

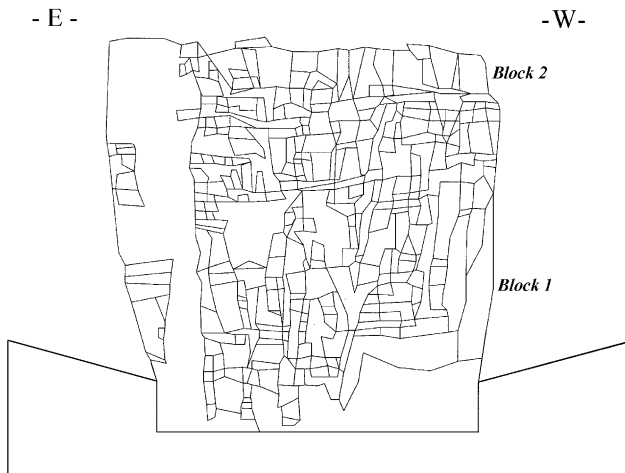


Fig. 13. Deterministic joint trace map of the terrace prepared using photogeological map of the upper terrace (Fig. 12) and the block cutting algorithm (DC) of Shi [1].

marching scheme in the solution process is very time consuming, even with today's fast computers. Therefore, the issue of the most relevant record should be resolved as much as possible before the analysis begins, on the basis of geological and seismological considerations. The CPU time would be spent more effectively in performance of sensitivity analyses for interesting geotechnical variables such as joint cohesion and friction angle, peak ground acceleration (PGA), and dimensions (length, spacing) of support elements. In the following sections the selection of the most appropriate input motion is discussed.

5.2. The Nuweiba earthquake record

In this research we chose to use the recorded time history of the $M_w = 7.1$ Nuweiba earthquake which occurred in November 1995 in the Gulf of Eilat (Aqaba) with an epicenter near the village of Nuweiba, Egypt. The main shock was recorded at the city of Eilat where the tremor was felt by people, and structural damage was detected in houses and buildings. The city of Eilat is located 91 km north from the epicenter and 186 km south of Masada, on the northern coast of the gulf of Eilat (Aqaba). Fig. 14 shows the vertical and EW components of the accelerogram that were recorded in Eilat. The PGA of the Nuweiba record as measured in Eilat was $0.09g$.

5.3. Incorporation of site effects

The Eilat seismological station is situated on a thick fill layer of Pleistocene alluvial fan deposits. The recorded accelerogram therefore represents the response of a site situated on deep fill layer rather than on sound bedrock. Therefore, direct application of the original Eilat record for the case of the Masada rock site would

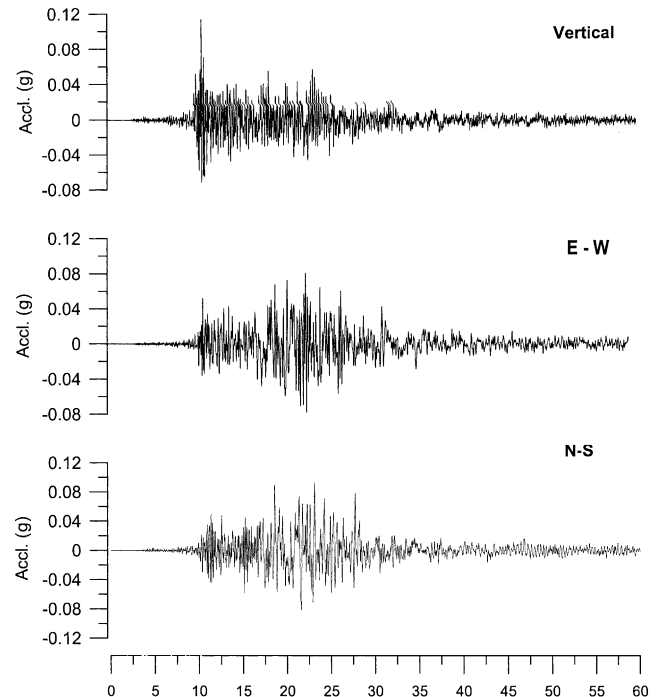


Fig. 14. Time history of the $M_w = 7.1$ Nuweiba earthquake (22 November 1995) as recorded at the city of Eilat on a thick fill layer of Pleistocene alluvial fan deposits.

be inappropriate. In order to obtain a “rock response” record for the Nuweiba event it would be necessary therefore to remove the local site effect of the fill layer, which typically amplifies ground motions, and to produce a corresponding “rock” response using an appropriate transfer function. This mathematical procedure is known as de-convolution.

In this research a one-dimensional multi layer model for the fill was utilized with the key parameters being shear wave velocity, thickness, and density for the horizontal fill layers. The material and physical parameters were determined using both seismic refraction survey data and down-hole velocity measurements. The appropriate transfer function was developed by optimization of both theoretical and experimental results [38]. The resulting de-convoluted record for rock response is shown in Fig. 15.

Although the Masada site is situated directly on rock, a significant topographic effect was recorded in the field [25,28], and it should therefore be considered in the development of the relevant input motion for the site. An empirical response function for Masada, developed on the basis of the field study discussed in Section 2.2 above, is shown in Fig. 16. Three characteristic modes are found at 1.06, 3.8, and 6.5 Hz. The resulting time history is shown in Fig. 17. The forward modeling is performed using the modified input motion shown in Fig. 17.

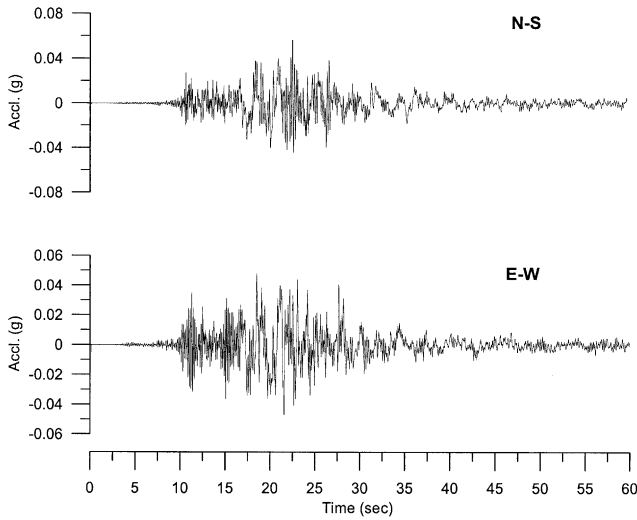


Fig. 15. De-convolution of the Eilat fill record (Fig. 14) for bedrock response.

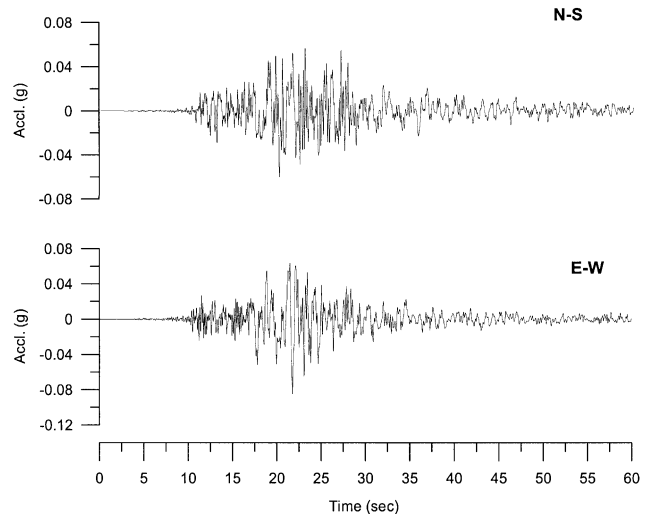


Fig. 17. The Nuweiba record modified for rock including topographic site effect.

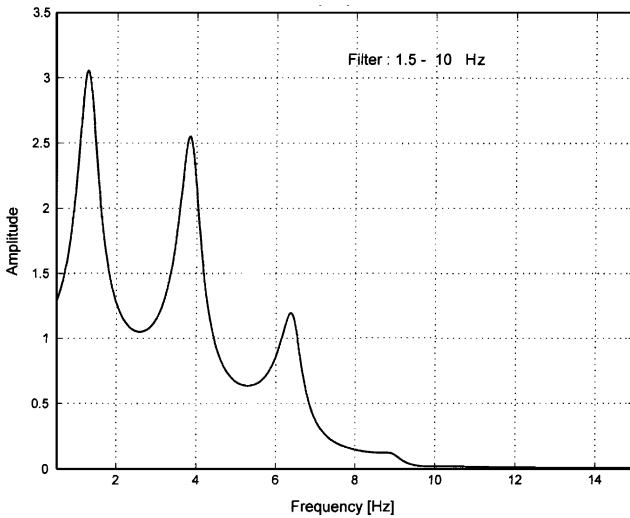


Fig. 16. An empirical response function for the topographic site effect at Masada.

6. Dynamic analysis

6.1. Numerical control parameters

The numerical control input parameters for DDA are the energy dissipation parameter ($K01$), the total number of time steps (n_s), the upper limit of time interval used in each time step (g_1), the assumed maximum displacement ratio (g_2) where (g_2) W is the assumed maximum displacement per time step and W is half the length of the analysis domain measured in the y direction, and the penalty or contact spring stiffness (g_0). Hatzor and Feintuch [6] explored the interrelationships between time step size (g_1) and assumed maximum displacement ratio (g_2) using comparison between DDA and analytical solutions for dynamic problems (block on

Table 2

Numeric control parameters for DDA

Total number of time steps	50,000
Time step size (g_1)	0.0002 s
Assumed maximum displacement ratio (g_2)	0.0015
Contact spring stiffness (g_0)	5×10^6 kN/m
Factor of over-relaxation	1.3

an incline subjected to dynamic load). Doolin and Sitar [39] and Tsesarsky et al. [9] further studied the role of time step size and penalty value (g_0) using comparison with analytical solutions and results of shaking table experiments, respectively. In this research the conclusions from these previous studies [6,9,39] are utilized for the selection of the most appropriate input numerical-control parameters, the values of which are listed in Table 2. Several comments about the selected time step size (g_1) and the energy dissipation parameter ($K01$) are further discussed below.

6.1.1. Time step size

The time step size affects the accuracy and efficiency of the numerical solution [6,9,39]. For problems with analytical solutions the optimal time step size can be determined accurately. Numerical solutions however are used in cases for which analytical solutions do not exist; for such problems the numerical control parameters must be determined in advance on the basis of previous experience and engineering judgment. One way to estimate the suitability of the selected time step size in DDA is to check the average number of iterations per time step (i_{av}) required for convergence.

The system of equilibrium equations (4) is solved for the displacement variables using “open–close” iterations: first, the solution is checked to see how well the

“no tension–no penetration” constraints are satisfied. If tension or penetration is found along any contact, the constraints are adjusted by selecting new locks and constraining positions, and modified versions of \mathbf{K} and \mathbf{F} are formed from which a new solution is obtained. This iteration process is repeated until no tension and no penetration is found along all of the block contacts.

A high number of iterations per time step (i_{av}) indicates poor convergence rate in each time step. This may adversely affect the accuracy of the solution. For the problem at hand, with a time step size of 0.002 s the typical number of iterations per time step was about 9.0, indicating a time step size much too large. With a time step size of 0.0002 s however the typical number of iterations per time step was between 2.7 and 3.14, indicating a much better convergence rate and possibly greater accuracy. Therefore, a time step size of 0.0002 s was used in all DDA runs presented here.

Note that in preliminary studies of this problem [36,37,40] the selected time step was set to $g_1 = 0.002$ s and a value of $n_5 = 25,000$ time steps was input in order to run the entire 50 s event. When the convergence rate is poor however, the DDA code is programmed to cut the time step automatically during the computation (the input value of g_1 being only an upper limit). In such cases the actual time computed (ΔT) may be shorter than $g_1 \times n_5$. This indeed was the case in previous runs. With $g_1 = 0.0002$ s the total time computed (ΔT) was very close to the 10 s target using $n_5 = 50,000$ time steps (see Table 4).

6.1.2. Energy dissipation parameter

DDA formulation is completely linear-elastic with no energy dissipation mechanisms other than the mechanical energy required for elastic deformation of contact springs, elastic deformation of intact block material, and frictional sliding along discontinuities, which is the main source of energy consumption. Consequently, no “artificial” damping is introduced in the mathematical formulation of DDA. While this is an honest mathematical approach, it is not entirely realistic because irreversible processes such as crushing of block material at contact points, or temporary resistance to sliding offered by asperities, are not modeled. Such energy dissipation mechanisms, loosely referred to as “damping”, must be active during block system deformation and if not modeled, DDA results should be expected to provide exaggerated displacements.

As mentioned in Section 1.3 above, comparisons between DDA and shaking table experiments for a single block on an incline subjected to dynamic loads [9] proved that with 0% kinetic damping ($K01 = 1$) DDA results over predicted block displacements by as much as 80%, while with 2% kinetic damping ($K01 = 0.98$) the numerical solution and physical test results converged. The Masada problem presented here consists of 344

individual blocks that interact with each other during dynamic loading. Clearly with no kinetic damping DDA output should be expected to be overly conservative and the predicted damage excessive. The question of exactly how much kinetic damping would be necessary for valid damage prediction in this multi-block case can only be answered by repeated trials and errors. In this research we ran the problem repeatedly for kinetic damping values of: $K01 = 1, 0.999, 0.99, 0.98, 0.975, 0.95$, corresponding to 0%, 0.1%, 1%, 2%, 2.5%, and 5% kinetic damping.

6.1.3. Time window for analysis

Consider the complete 50 s record shown in Fig. 17. Using the optimal time step size for this problem (0.0002 s), a total number of 250,000 time steps would be required to complete the computation of the entire event from $t_0 = 0$, to $t_f = 50$ s. Such an analysis would take more than a week to complete, even with a fast computer, and would yield an extremely large data output file (approximately 150 Mb per a single run), making data handling and processing an elaborate task. Since the value of the selected time step size could not be compromised, we decided to focus the analysis on the 10 most critical seconds in the record, from $t_0 = 15$ to $t_f = 25$ s. Therefore, $n_5 = 50,000$ time steps was used as input to compute the complete 10 s time window. The average CPU time per run on a P4-1.5 GHz processor with 128 Mb RAM was typically 36 h. The typical size of the data output file for a single run was 28 Mb. With the specified time step size of $g_1 = 0.0002$ s the total time of the analysis was very close to $\Delta T = 10$ s (see Table 4).

6.1.4. Mechanical input parameters

The mechanical input parameters were based on the laboratory experiments described in Section 3 above. The joints were assumed cohesionless and with zero tensile strength. The assumed friction angle on all joints was set to 41° based on the direct shear test results that were performed on natural bedding planes. The values of elastic modulus and Poisson’s ratio for intact rock material were taken directly from the uniaxial compression tests described in Section 3. Table 3 summarizes the selected mechanical input parameters for the analysis.

Table 3
Material properties for rock at Masada

Unit weight of rock (γ)	25 kN/m ³
Elastic modulus (E)	43×10^6 kN/m ²
Poisson’s ratio (ν)	0.184
Friction angle of all discontinuities (ϕ)	41°
Cohesion of all discontinuities (C)	0
Tensile strength of all discontinuities (σ_t)	0

Table 4
Matrix of all DDA runs for the 10 s critical time window from $t_0 = 15$ s to $t_f = 25$ s

PGA (g)	Earthquake file	Kinetic damping (%)	Data output file	Graphic file	ΔT (s)	i_{av}	Figure
0.06	Tp10c	0	Dtt10c1	Dgt10c1	9.91	2.69	18A
0.06	Tp10c	2.5	Dtt10c75	Dgt10c75	9.99	3.08	18B
0.06	Tp10c	5	Dtt10c95	Dgt10c95	9.99	3.13	18C
0.2	Tp10c02g	0.1	Dt02g999	Dg02g999	9.87	2.91	
0.2	Tp10c02g	1	Dtc02g99	Dgc02g99	9.95	3.02	19A
0.2	Tp10c02g	2	Dtc0298	Dgc0298	9.99	3.06	19B
0.2	Tp10c02g	2.5	Dtc02975	Dgc02975	9.98	3.08	
0.2	Tp10c02g	5	Dt10c02g	Dgc02g95	9.99	3.03	
0.6	To10c06g	1	Dtc06g99	Dgc06g99	9.77	3.06	
0.6	To10c06g	2	Dtc0698	Dgc0698	0.99	3.04	
0.6	To10c06g	2.5	Dtc06975	Dgc06975	9.98	3.09	
0.6	To10c06g	5	Dt10c06g	Dg10c06g	9.98	3.14	
1.0	Tp10c1g	1	Dtc1g99	Dgc1g99	9.72	3.06	
1.0	Tp10c1g	2	Dtc981g	Dgc981g	10	3.05	19C
0.6	To10c06g	2	Dtb7006g	Dgb7006g	9.989	3.10	20A
0.6	To10c06g	2	Dt70b06g	Dg70b06g	9.989	3.06	20B

ΔT is the total time computed by DDA after 50,000 time steps; i_{av} is the average number of iterations per time step.

6.2. Results of dynamic analysis

The critical 10 s of the earthquake were computed using the modified rock response record (Fig. 17) with different amounts of kinetic damping. The response of the studied terrace to stronger events was studied by scaling the original record to PGA values of 0.2g, 0.6g, and 1g. Table 4 summarizes all DDA runs with the actual time calculated (ΔT) and the average number of iterations per time step (i_{av}).

7. Discussion

7.1. The influence of energy dissipation on DDA output

In Fig. 18A the results of DDA computation for the modified rock response record (Fig. 17) is shown for time window $t_0 = 15$ to $t_f = 25$ s for a computation with no energy dissipation, or with zero kinetic damping. The resulting damage is devastating and the terrace completely disintegrates. Recall that the peak horizontal ground acceleration (PGA) for the record was only 0.06g (Fig. 17). On the basis of historical and seismological evidence (Section 2 above) we believe that the terrace must have been subjected to many events of greater intensity since Herod fortified it, yet it remained largely intact during its 2000 years of recorded history. Therefore, the damage presented in Fig. 18A must be considered excessive and unrealistic. From the output shown in Fig. 18A it clearly seems that a certain amount of energy dissipation must be considered to truly simulate the performance of a jointed rock slope subjected to dynamic loading.

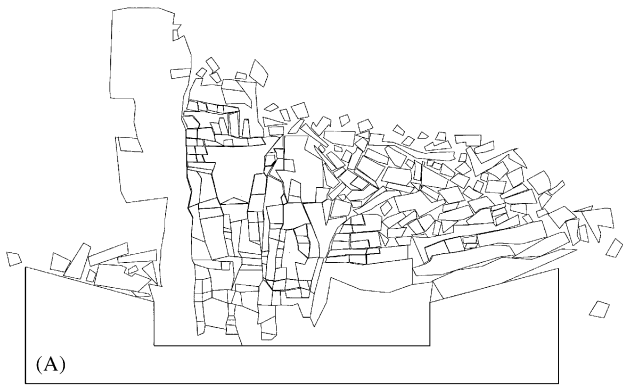
In Figs. 18B the same record is computed but with 2.5% kinetic damping. Introduction of a relatively small amount of energy dissipation drastically reduces the computed damage for the terrace, and with further energy dissipation (5%, Fig. 18C) the damage is further restrained.

Judging from the output shown in Fig. 18 it does not seem justified to introduce 5% kinetic damping (Fig. 18C), since even with 2.5% damping the terrace remains largely intact (Fig. 18B). The shaking table validation study [9] showed that with 2% kinetic damping DDA and experimentally obtained displacements of a single block converged (Fig. 2). The results of the analyses shown in Fig. 18 suggest that the similar amount of damping may be required in dynamic analysis of a multi-block case.

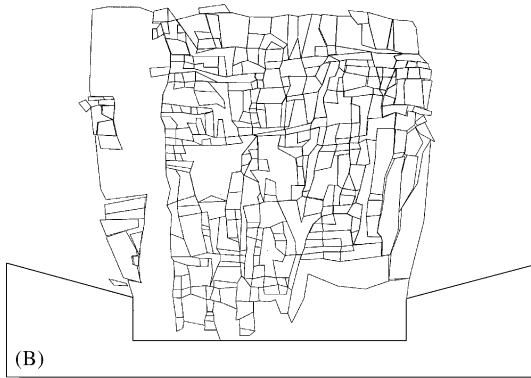
7.2. Energy dissipation calibration and DDA validation

With the required energy dissipation parameter in DDA roughly estimated, we may proceed to try and evaluate it more accurately using further analysis. According to the Israel building code—Israel Standard 413, the Dead Sea valley has been classified as a region in which earthquake-induced peak horizontal ground acceleration (PGA) exceeding 0.2g at the bedrock level is expected with a 10% probability within any 50-year window. This is analogous to a 475-year average recurrence interval for such acceleration.

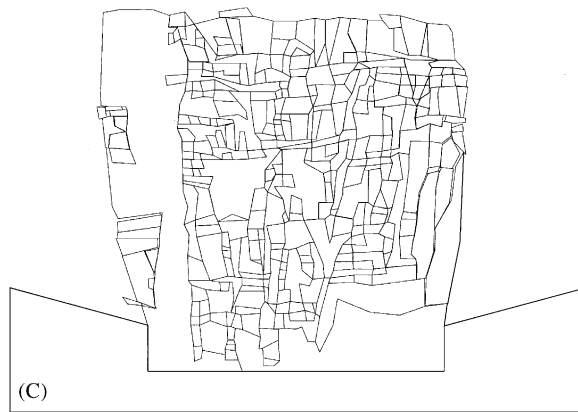
The upper terrace of the palace is still standing since Herod's construction phase more than 2000 years ago. We should therefore anticipate that the predicted damage by DDA for a PGA=0.2g event should be minimal, because the terrace with its fortification has probably experienced several similar events since it was



(A)



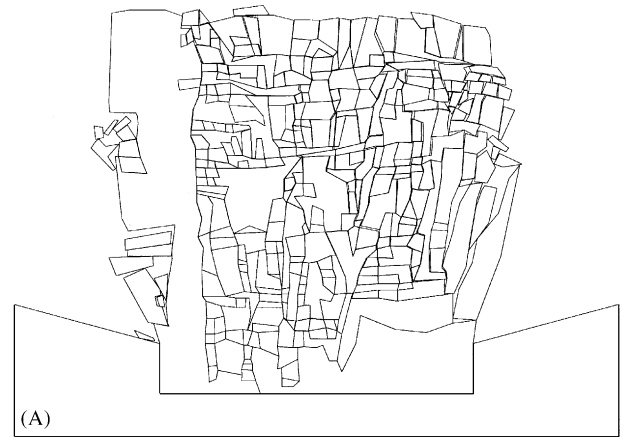
(B)



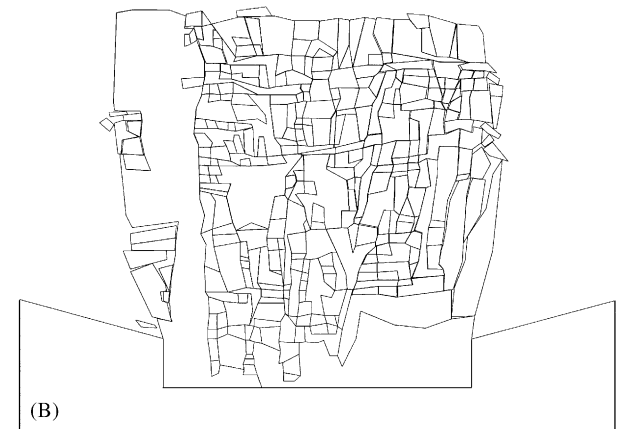
(C)

Fig. 18. Results of dynamic DDA modeling for the modified Nuweiba record: (A) no energy dissipation; (B) 2.5% kinetic damping; and (C) 5% kinetic damping.

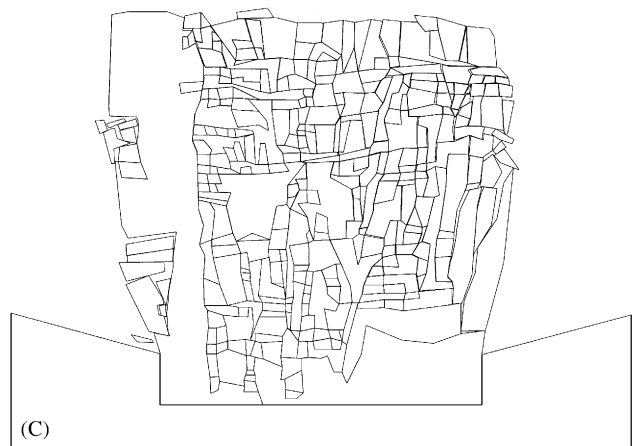
built. In order to simulate a $PGA = 0.2g$ event we scaled the modified record (Fig. 17) by multiplying all x , y , z acceleration components by: $0.2/PGA_{\text{original}}$. Fig. 19A and B show the predicted damage after 10 s of shaking under the original record when scaled to $PGA = 0.2g$, with 1% and 2% kinetic damping, respectively. Since the upper terrace is still standing, the graphic output shown in Fig. 19A seems excessive as a deep, open fissure transects the terrace from the bottom right to the top left, forming a stepped base dipping 45° to the west. Naturally, with this amount of damage the terrace



(A)



(B)



(C)

Fig. 19. Results of dynamic DDA modeling for the modified Nuweiba record scaled to $PGA = 0.2g$: (A) 1% kinetic damping; (B) 2% kinetic damping; and (C) modified Nuweiba record scaled to $PGA = 1g$ with 2% kinetic damping.

cannot be considered safe in the long-term as it would be prone to repeated toppling failures at the west face.

The damage after 10 s of shaking with 2% damping however (Fig. 19B) seems tolerable and the terrace, which remains largely intact, may be considered stable in the long term.

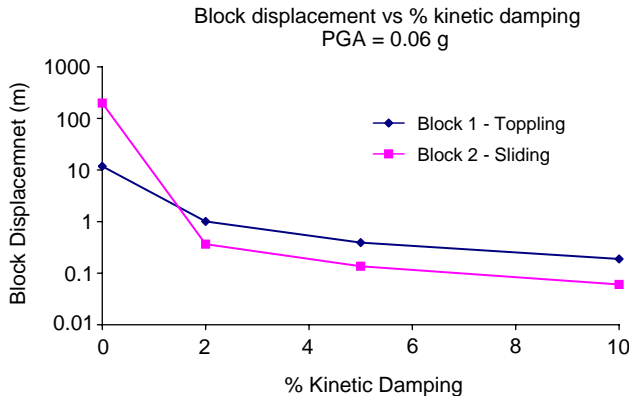


Fig. 20. Block displacement after 10s of shaking with different amount of kinetic damping. Block 1—at the toe of the west face, Block 2—at the top of the west face. Input earthquake record scaled to horizontal PGA = 0.2g.

In Fig. 20 the displacement of two critical keyblocks at the west face after 10s of shaking are plotted for kinetic damping values of 0%, 1%, 2%, 5%, and 10%. Block 1 at the toe of the slope exhibits toppling deformation while block 2, at the top of the west slope exhibits sliding deformation (for block location see Fig. 13). The keyblock displacement output in Fig. 20 may be used as a guideline for establishing a slope stability criterion. With nil to 2% damping both blocks are unstable and will eventually fail. However, with damping values greater than roughly 2% the keyblocks blocks may be considered stable. The stability of the keyblocks is not improved significantly with increasing kinetic damping.

We may therefore conclude that as in the case of a single block, 2% kinetic damping is the correct number for the multiple block case in DDA as well. Thus the applicability of DDA for dynamic analysis of jointed rock slopes is confirmed, provided that the correct amount of energy dissipation is used. It must be noted however that this result is strictly valid for DDA only.

7.3. The influence of acceleration magnitude on DDA output

Fig. 19C shows the predicted damage at the terrace when the record is further scaled to 1.0g. Surprisingly, the damage does not seem to be much greater as one would expect. Naturally, with acceleration levels of 1g blocks at the upper row in the terrace may be expected to lift in the air for very short time spans when the scaled accelerations attain a level of 1g. It should be noted that the frequency content was not altered in the scaled records as all acceleration components were multiplied by a scalar only. It is not possible to check the validity of this result of DDA because we do not know what was the maximum PGA that developed at Masada in the

past 2000 years. Intuitively however the result in Fig. 19C seems to underestimate the expected damage in a 1.0g PGA earthquake.

The reason for the apparently underestimated damage under high acceleration magnitudes could be related to the way in which energy dissipation is currently implemented in DDA. It would be instructive to test the same loading configuration but with a more rigorous damping algorithm (perhaps a spring + dashpot model at contact points) and to check if the terrace sustains the high loads in the same manner as shown in Fig. 19C.

7.4. The influence of rock bolt reinforcement

Modeling bolting reinforcement is straightforward in the DDA method and the implementation of strain energy for bolting connections is discussed in detail by Shi [1,2]. Yeung [41,42] and Yeung and Goodman [43] demonstrated bolting reinforcement for underground problems using DDA and discussed its potential for general applications. In this case two rock bolting configurations are modeled:

- Bolt length = 6 m, spacing = 2 m, stiffness = 24×10^4 kN/m², both west and east faces (Fig. 20A).
- Bolt length = 6 m, spacing = 4 m, stiffness = 24×10^4 kN/m², only west face (Fig. 20B).

The modeled bolts were not pre-tensioned. The block mesh with the different bolting patterns was subjected to the modified record normalized for PGA = 0.6g for the same 10s time window used in previous analyses, and with the same time step size of 0.0002 s (see Table 4).

The effect of rock bolting is apparent. With the dense bolting pattern the terrace remains virtually intact after 10s of shaking with PGA = 0.6g, and all the blocks remain in place. With the sparse bolting pattern which was limited to the west face only, the damage in the east face is identical to that which was detected in the same run but with no bolting (Fig. 19C). In the west face however local block failures are detected. The effectiveness of bolting reinforcement in jointed rock masses is evident from the output in Fig. 21.

7.5. Limitations of the DDA model

We have shown in this paper that a dynamic DDA analysis performed with proper numerical control parameters is capable of predicating both failure modes and amount of damage in a discontinuous rock slope subjected to dynamic loading. However several limitations must be considered:

- (1) In this study we used a two-dimensional solution for a three-dimensional problem. A three-dimensional code that can solve this problem which

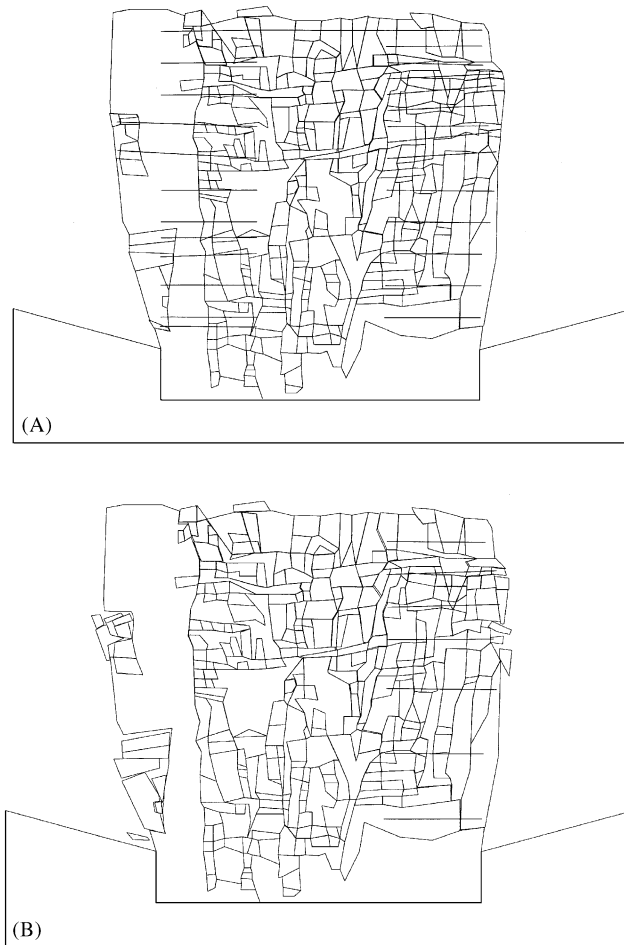


Fig. 21. Performance of the rock slope with rock bolt reinforcement. Modified Nuweiba record with 2% kinetic damping scaled to $PGA = 0.6g$: (A) dense bolting pattern; and (B) sparse bolting pattern.

consists of several hundred blocks is not available for us at present and therefore a two-dimensional solution was applied. Since the slope is exposed on both sides (east and west), a two-dimensional approximation should be reasonable. Nevertheless, lateral block reinforcement provided by the third dimension (into the slope) is ignored by the analysis. This shortcoming may be responsible for the excessive damage that was predicted by DDA with zero kinetic damping. Therefore, the 2% damping criterion may reflect this limitation. Perhaps with a three-dimensional configuration a smaller amount of damping will be required.

- (2) The damping mechanism we used is “kinetic” damping which is not a physically valid damping mechanism. Introduction of a physical damping mechanism, for example a spring + dashpot model at contact points would most certainly provide more accurate results. However, with a proper damping mechanism the correct value of the damping coefficients still remains an open question.

- (3) In the DDA model used here the blocks are simply deformable, namely stress and strain distributions through the blocks are not computed, and all stresses and strains are identical everywhere in the block. This simplification becomes problematic in high stress problems, in rock masses consisted of soft block material, and where the block shapes are irregular. In the case of Masada the problem is clearly a “low stress” problem and the block material is extremely stiff and therefore the simply deformable blocks assumption is justified. Nevertheless, many blocks in the computed cross section have irregular geometries which may lead to numeric errors when the simply deformable blocks assumption is used.

8. Conclusions

- The rock terrace under King Herod’s Palace has experienced several shaking events with PGA of about $0.2g$ since the palace was built it was fortified more than 2000 years. Nevertheless, the foundations at the top edge of the terrace are still standing. This historical constraint is utilized for calibration of a dynamic DDA model which uses as input a typical earthquake record for the Dead Sea rift system scaled to $PGA = 0.2g$.
- In order to model dynamic deformation of jointed rock slopes every attempt should be made to determine as accurately as possible the mechanical properties of the rock mass, the geometry of the rock structure, and the expected style of dynamic loading.
- The time step size used in the solution process effects the convergence rate and should be selected carefully. For DDA we find that a small time step size is preferable, even if the total length of the analysis time must be compromised.
- By the comparison with historical evidence we conclude that some energy dissipation must be introduced to the otherwise un-damped DDA formulation in order to account for non-linear, inelastic process which may take place during shaking at block contacts. The required amount of kinetic damping seems to be in the order of 2%, based on both shaking table experiments and field scale performance. This value is strictly valid for DDA and must be determined separately for each distinct element code.
- The selected amount of damping may also compensate for the two-dimensional simplification where lateral block reinforcement is neglected.
- Under high accelerations DDA output seems to underestimate dynamic displacements. This problem could be associated with the method in which energy dissipation is currently modeled in DDA.

- In this research we performed calibration of the numerical control parameters by comparison between numerical modeling output and field scale performance. Such calibration is un-avoidable, and is required in all other methods as well. However, once the numerical control parameters are calibrated within the range of validity of this calibration, investigation can proceed with different or more complex problems, utilizing the power of the numerical tool.
- Bolting reinforcement is shown to be efficient in stabilization of jointed rock slopes that are subjected to dynamic loads.

Acknowledgements

This research was funded by Israel Nature and Parks authority and partially by the US–Israel Bi-national Science Foundation (BSF) through grant 98-399. The support of the two agencies is hereby acknowledged. Dr. Gen-Hua Shi is thanked for making his dynamic DDA code available for this study. M. Tsesarsky is thanked for collecting and synthesizing structural data in the field and for assistance with direct shear tests. Dr. V. Palchik is thanked for digitizing the structural trace map of the upper terrace. Dr. Guy Stiebel is thanked for guiding us on Masada with archeological insights and for providing the 1924 aerial photographs. Finally, Professor Hudson and two anonymous reviewers are thanked for their critical reading of the manuscript and for their thoughtful comments.

References

- [1] Shi G-H. Block system modeling by discontinuous deformation analysis. Southampton, UK: Computational Mechanics Publications; 1993. p. 209.
- [2] Shi G-H. Discontinuous deformation analysis: a new numerical model for the statics and dynamics of block systems. Ph.D. thesis, University of California, Berkeley, 1988.
- [3] Amadei B, Lin C, Dwyer J. Recent extensions to the DDA method. In: Salami MR, Banks D, editors. Proceedings of the First International Forum on DDA and Simulations of Discontinuous Media. Albuquerque: TSI Press; 1996. p. 1–30.
- [4] Jing L. A review of techniques, advances and outstanding issues in numerical modeling for rock mechanics and rock engineering. Int J Rock Mech Min Sci 2003;40:283–353.
- [5] Shi G-H. Single and multiple block limit equilibrium of key block method and discontinuous deformation analysis. In: Hatzor YH, editor. Stability of rock structures: Proceedings of the Fifth International Conference of Analysis of Discontinuous Deformation. Lisse: Balkema Publishers; 2002. p. 3–43.
- [6] Hatzor YH, Feintuch A. The validity of dynamic displacement prediction using DDA. Int J Rock Mech Min Sci 2001;38(4): 599–606.
- [7] MacLaughlin MM. Discontinuous deformation analysis of the kinematics of landslides. Ph.D. dissertation, Department of Civil and Env. Engineering, University of California, Berkeley, 1997.
- [8] Wartman J, Bray JD, Seed RB. Inclined plane studies of the Newmark sliding block procedure. J Geotech Geoenviron Eng, ASCE 2003;129(8):673–84.
- [9] Tsesarsky M, Hatzor YH, Sitar N. Dynamic block displacement prediction—validation of DDA using analytical solutions and shaking table experiments. In: Hatzor YH, editor. Stability of rock structures: Proceedings of the Fifth International Conference of Analysis of Discontinuous Deformation. Lisse: Balkema Publishers; 2002. p. 195–203.
- [10] McBride A, Scheele F. Investigation of discontinuous deformation analysis using physical laboratory models. In: Bicanic N, editor. Proceedings of the ICADD-4, Fourth International Conference of Analysis of Discontinuous Deformation, Glasgow, Scotland, UK, 2001.
- [11] Garfunkel Z, Zak I, Freund R. Active faulting in the Dead Sea Rift. Tectonophysics 1981;80:1–26.
- [12] Garfunkel Z, Ben-Avraham Z. The structure of the Dead Sea basin. In: Dynamics of extensional basins and inversion tectonics. Tectonophysics 1996;266:155–76.
- [13] Niemi TM. The Dead Sea. In: Ben Avraham Z, Gat JR, editors. The lake and its setting. Oxford, London: Oxford University Press Ltd.; 1997. p. 286.
- [14] Shapira A. A probabilistic approach for evaluating earthquake risk with application to the Afro-Eurasian junction. Tectonophysics 1983;95:75–89.
- [15] Shapira A, van Eck T. Synthetic uniform hazard site specific response spectrum. Nat Hazard 1993;8:201–5.
- [16] Ben-Menahem A. Earthquake catalog for the Middle East. Boll Geofis Teor Appl 1979;XXI:245–313.
- [17] Turcotte T, Arieh E. Catalog of earthquakes in and around Israel, Appendix 2.5A in: Shivta site Preliminary Safety Analysis Report, Israel Electric Corp. Ltd., 1988.
- [18] Amiran DHK, Arieh E, Turcotte T. Earthquakes in Israel and adjacent areas: macro-seismicity observations since 100BCE. Isr Explor J 1994;41:261–305.
- [19] Netzer E. Masada III—the Yigael Yadin excavations 1963–1965 Final Reports—the buildings stratigraphy and architecture, Israel Exploration Society, The Hebrew University, Jerusalem, Israel, 1991, 665pp.
- [20] Davis LL, West LR. Observed effects of topography on ground motion. Bull Seismol Soc Am 1973;63:283–98.
- [21] Celebi M. Topographical and geological amplifications determined from strong-motion and aftershock records of the 3 Mach 1985 Chile earthquake. Bull Seismol Soc Am 1987;77:1147–67.
- [22] Chavez-Garcia FJ, Sanchez LR, Hatzfeld D. Topographic site effects and HVSR—a comparison between observations and theory. Bull Seismol Soc Am 1996;86:1559–73.
- [23] Bouchon M, Barker JS. Seismic response of a hill: the example of Tarzana, CA. Bull Seismol Soc Am 1996;86:66–72.
- [24] Ashford SA, Sitar N, Lysmer J, Deng N. Topographic effects on the seismic response of steep slopes. Bull Seismol Soc Am 1997;87:701–9.
- [25] Zaslavsky Y, Shapira A. Experimental study of topographic amplification using the Israel seismic network. J Earthquake Eng 2000;4(1):43–65.
- [26] Bard PY, Tucker BE. Underground and ridge and site effects: comparison of observation and theory. Bull Seismol Soc Am 1985;75:905–22.
- [27] Sanchez-Sesma FJ, Campillo M. Diffraction of P, SV and Rayleigh waves by topographic features: a boundary integral formulation. Bull Seismol Soc Am 1991;81:2234–53.
- [28] Zaslavsky Y, Shapira A, Arzi AA. Earthquake site response on hard rock—empirical study. In: Hatzor YH, editor. Stability of rock structures: Proceedings of the Fifth International Conference of Analysis of Discontinuous Deformation. Lisse: Balkema Publishers; 2002. p. 133–44.

- [29] Geli L, Bard PY, Jullien B. The effect of topography on earthquake ground motion: a review and new results. *Bull Seismol Soc Am* 1988;78:42–63.
- [30] Zaslavsky Y, Shapira A, Arzi AA. Amplification effects from earthquakes and ambient noise in Dead Sea Rift (Israel). *Soil Dyn Earthquake Eng* 2000;20(1–4):187–207.
- [31] Hatzor YH, Palchik V. The influence of grain size and porosity on crack initiation stress and critical flaw length in dolomites. *Int J Rock Mech Min Sci* 1997;34(5):805–16.
- [32] Hatzor YH, Palchik V. A microstructure-based failure criterion for Aminadav dolomites—Technical Note. *Int J Rock Mech Min Sci* 1998;35(6):797–805.
- [33] Palchik V, Hatzor YH. Crack damage stress as a composite function of porosity and elastic matrix stiffness in dolomites and limestones. *Eng Geol* 2002;63:233–45.
- [34] Hatzor YH. Keyblock stability in seismically active rock slopes—the Snake Path cliff—Masada. *J Geotech Geoenviron Eng ASCE* 2003;129(8):697–710.
- [35] Goodman RE, Shi G-H. *Block theory and its application to rock engineering*. Englewood Cliffs, NJ: Prentice-Hall; 1985.
- [36] Hatzor YH. Dynamic rock slope stability analysis at Masada national monument using Block Theory and DDA. In: Amadei B, Kranz R, Scott GA, Smeallie PH, editors. *Rock mechanics for industry*, Proceedings of the 37th US Rock Mechanics Symposium. Rotterdam: Balkema; 1999. p. 63–70.
- [37] Hatzor YH. Natural rock-slope stability issues at Masada national monument a case study. In: Vouille G, Berest P, editors. *Proceedings of the Ninth ISRM Congress*, vol. 3. Lisse: Balkema; 1999. p. 1621–8.
- [38] Zaslavsky Y, Shapira A. Questioning nonlinear effects in Eilat during MW = 7.1 Gulf of Aqaba earthquake, Proceeding of the XXVII General Assembly of the European Seismological Commission (ESC), Lisbon, Portugal, September 10–15, 2000. p. 343–47.
- [39] Doolin DM, Sitar N. Displacement accuracy of discontinuous deformation analysis method applied to sliding block. *J Eng Mech* 2002;128(11):1158–68.
- [40] Hatzor YH, Arzi AA, Tsesarsky M. Realistic dynamic analysis of jointed rock slopes using DDA. In: Hatzor YH, editor. *Stability of rock structures: Proceedings of the Fifth International Conference of Analysis of Discontinuous Deformation*. Lisse: Balkema Publishers; 2002. p. 47–56.
- [41] Yeung MR. Application of Shi's discontinuous deformation analysis to the study of rock behavior. Ph.D. thesis, University of California, Berkeley, 1995.
- [42] Yeung MR. Analysis of a mine roof using the DDA method. *Int J Rock Mech Min Sci* 1993;30(7):1411–7.
- [43] Yeung MR, Goodman RE. Multi block stability analysis using the DDA method. In: Myer LR, Cook NGW, Goodman RE, Tsang C-F, editors. *Fractured and jointed rock masses*. Rotterdam: Balkema; 1995. p. 701–7.